Geophysical Research Letters

RESEARCH LETTER
10.1029/2022GL098034

Key Points:

- The circulation pattern (P5) most conducive to the occurrence of daily precipitation extremes is identified using self-organizing map
- Seven out of total 11 days in the "21·7" and "75·8" catastrophic extreme precipitation events belong to P5 pattern
- The dynamical processes, that is, the stronger ascending motions, dominate the more-intense precipitation extremes in P5 pattern

Supporting Information:

Supporting Information may be found in the online version of this article.

Correspondence to:

B. Liu,
boliu@cug.edu.cn

Citation:

Zhang, S., Chen, Y., Luo, Y., Liu, B., Ren, G., Zhou, T., et al. (2022). Revealing the circulation pattern most conducive to precipitation extremes in Henan Province of North China. *Geophysical Research Letters*, *49*, e2022GL098034. https://doi.org/10.1029/2022GL098034

Received 24 JAN 2022
Accepted 26 MAR 2022

Revealing the Circulation Pattern Most Conducive to Precipitation Extremes in Henan Province of North China

Sihan Zhang[1], Yangruixue Chen[2], Yali Luo[3], Bo Liu[1,4], Guoyu Ren[1,4,5], Tianjun Zhou[6], Cristian Martinez-Villalobos[7,8], and Meiyu Chang[1]

[1]Department of Atmospheric Science, School of Environmental Studies, China University of Geosciences, Wuhan, China, [2]Plateau Atmosphere and Environment Key Laboratory of Sichuan Province, School of Atmospheric Sciences, Chengdu University of Information Technology, Chengdu, China, [3]State Key Laboratory of Severe Weather, Chinese Academy of Meteorological Sciences, Beijing, China, [4]Centre for Severe Weather and Climate and Hydro-geological hazards, Wuhan, China, [5]Laboratory for Climate Studies, National Climate Center, China Meteorological Administration, Beijing, China, [6]LASG, Institute of Atmospheric Physics, Chinese Academy of Science, Beijing, China, [7]Faculty of Engineering and Science, Universidad Adolfo Ibañez, Santiago, Chile, [8]Data Observatory Foundation, Santiago, Chile

Abstract Two catastrophic extreme precipitation events in July 2021 and August 1975 caused tremendous damages and deaths in Henan, one of the most populated provinces in China. Revealing the relationship between large-scale circulation patterns and precipitation extremes is vital for understanding the physical mechanisms and providing potential value for improving prediction and hence reducing impacts. Here, nine large-scale circulation patterns are identified for July–August using the self-organizing map. We find daily precipitation extremes under the fifth pattern (P5), characterized with the strongest easterly wind anomalies in Henan, feature the highest frequency and the largest intensity. Seven out of total 11 days in the two catastrophic extreme precipitation events belong to P5, and the top two maximum hourly precipitation extremes over continental China occurred under P5. The larger intensity of precipitation extremes is attributed to the dynamical contribution, suggesting more-intense precipitation extremes under P5 are largely dominated by stronger ascending motions.

Plain Language Summary Henan is one of the most populated provinces in China. Two catastrophic extreme precipitation events in July 2021 and August 1975 caused devastating catastrophes, such as flooding and urban waterlogging, which resulted in widespread impacts on agricultural production, human livelihood, and economic development. We used a clustering method called self-organizing map to link large-scale circulation patterns with daily precipitation extremes in Henan Province. Our results show that the fifth pattern (P5), associated with the strongest easterly wind anomalies over Henan Province, is most conducive to extreme rainfall. Precipitation extremes under P5 exhibit the highest occurrence frequency and the largest mean intensity. Seven out of total 11 days for the two catastrophic extreme precipitation events belong to P5, while the top two maximum hourly precipitation extremes over continental China occurred under P5. The larger mean intensity of precipitation extremes under P5 is mainly caused by strong ascending motions. This work provides important implications for understanding the physical mechanisms and also providing potential value for the forecasting of precipitation extremes in Henan Province.

1. Introduction

With the enhancement of the East Asian Summer Monsoon, a rain belt over North China usually begins during mid-July, lasting for about 1 month (Ding & Chan, 2005). Though the annual accumulated rainfall is relatively lower, daily or hourly precipitation extremes associated with this rain belt in North China are comparable or even larger than those in South China or Southwest China (Figure 1b; Ding & Zhang, 2009; Luo et al., 2016; Wu & Luo, 2019). Indeed, the top two maximum hourly rainfall over continental China are recorded at Zhengzhou station (201.9 mm, 20 July 2021) and Linzhuang station (198.5 mm, 5 August 1975). Both stations are located in Henan Province, which is located to the east of the Taihang Mountains and the Funiu Mountain (Figure 1d). These two hourly precipitation extremes belong to two catastrophic consecutive rainfall events—the "21·7" (from 17th to 22nd, July 2021; e.g., Zhang et al., 2021) and "75·8" (from 4th to 8th, August 1975; e.g., Ding, 2015) events, respectively. Due to Henan Province being one of the main grain production areas and populated provinces in China (Figure 1a), devastating catastrophes such as flooding and urban waterlogging induced

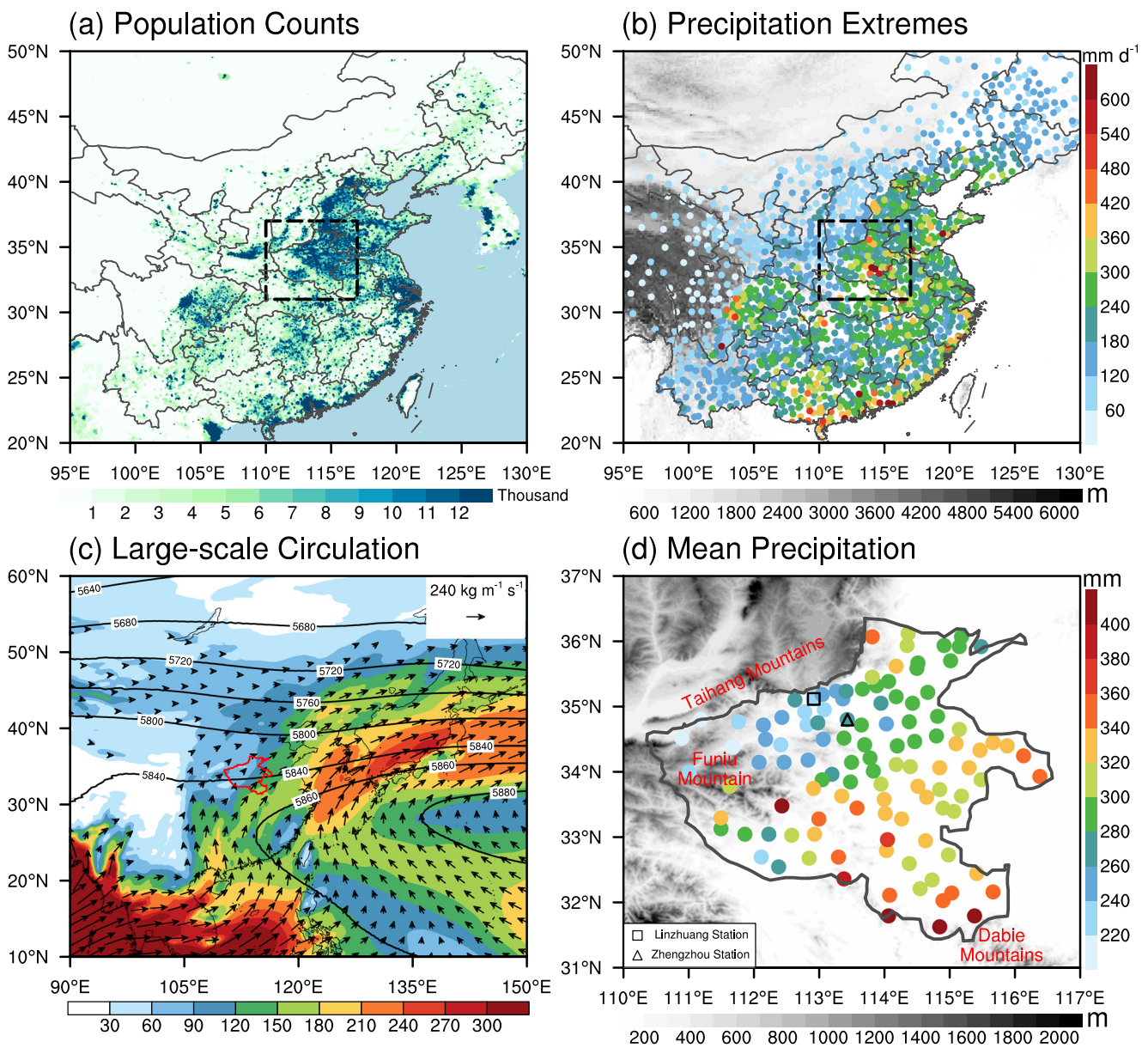

Figure 1. (a) Spatial distribution of population counts (colored shading, unit: thousand per 0.0417° × 0.0417°) in 2020 from the Gridded Population of the World Version 4. (b) Spatial distribution of the maximum daily precipitation (colored dots; units: mm day $^{-1}$). (c) The averaged geopotential height (contours; unit: gpm) at 500 hPa and column-integrated moisture flux (arrows; units: kg·m^{-1} ·s^{-1}) in July and August. (d) Spatial distribution of mean July–August total precipitation (colored dots; units: mm) over Henan Province. The shadings in (b and d) represent the topography (units: m), and in (c) the shading indicates the amount of moisture flux.

by extreme precipitation have profound impact on agricultural production, human livelihood and economic development (Ding, 2015). For example, the "21·7" event has led to more than 300 people deaths and $18 billion economic damages, and the "75·8" event caused more than 26 thousand deaths and $1.5 billion economic losses (Ding, 2015; Shi et al., 2021). Thus, it is important to better understand the physical mechanisms explaining occurrences of precipitation extremes over Henan Province.

Many previous studies have emphasized the importance of large-scale circulation patterns on heavy precipitation events over North China (Chen & Zhang, 2020; Zhao et al., 2019). Based on the analysis of 33 extreme precipitation events during 1958–1976 over North China, Ding et al. (1980) found that persistent extreme precipitation mainly occurs under a long-lived meridional circulation with a "high to the east and low to the west" or a "two-high" pattern, which is favorable for not only the maintenance of synoptic-scale systems, such as low-level

vortex, shear line, cold front with a trough and occasionally typhoon, but also the establishment of steady moisture channels. Such synoptic environments are conducive to the initiation and development of mesoscale convective systems, which are directly linked to the precipitation processes. For example, low-level jets could produce strong convergence by enhancing orographic lifting to initiate local convection over North China (Sun et al., 2012; Xia & Zhang, 2019). Indeed, both the "21·7" and "75·8" extraordinary rainfall events happened under extremely favorable and steady large-scale circulation patterns, with two high systems, around the Qinghai and the Sea of Japan, respectively, and a southeasterly or easterly moisture jet strengthened by a typhoon. Combined with the topographic blocking effect from the Funiu Mountain and Taihang Mountains, mesoscale convective activity is easily triggered and maintained in Henan Province, resulting in both extreme precipitation events (Ding, 2015; Shi et al., 2021; Zhang et al., 2021). Therefore, revealing the relationship between large-scale circulations and precipitation extremes is important for advancing the understanding of the physical mechanisms and providing potential value for the prediction of precipitation extremes in this region.

Clustering of the large-scale circulation patterns and further identification of the pattern(s) most likely to induce heavy rainfall is a well-established method for the understanding of the association between circulations and precipitation extremes (Ohba et al., 2015). As a nonlinear cluster technique, the self-organizing map (SOM) is an unsupervised neural network method with no a priori assumption that can be used to identify the complex relationships among nonlinear meteorological variables and, in some cases, precursors to extreme events (Kohonen, 1995; Ohba et al., 2015). Moreover, physical scaling diagnostic has been proved to be effective in decomposing changes of extreme precipitation into dynamic and thermodynamic contributions to understand the mechanisms of precipitation extremes at play and real the scaling relation in reproducing the spatial pattern of precipitation extremes and associated changes (Chang et al., 2020, 2021; O'Gorman & Schneider, 2009; Pfahl et al., 2017). In this study, we aim to combine the SOM technique and the physical scaling diagnostic to investigate the relationship between circulation patterns and daily precipitation extremes in Henan Province with the emphasis on the identification of the circulation patterns most conducive to extreme rainfall and the underlying mechanisms.

The rest of this paper is organized as follows. Section two describes the data and methodology, including the SOM method and physical scaling diagnostic of precipitation extremes. Section three presents the clustering of large-scale circulation patterns and the relationship between circulation patterns and daily precipitation extremes. Section four reveals the potential mechanisms involved in the differences of precipitation extremes among these circulation patterns. Section five provides the discussions and concluding remarks.

2. Data and Methodology

2.1. Observed and Reanalysis Data Sets

Observed daily precipitation data from 112 stations in Henan Province for the period 1970–2021 is obtained from the National Meteorological Information Center, China Meteorological Administration (CMA). The daily precipitation is accumulated from 1200 Coordinated Universal Time (UTC) in the previous day to 1200 UTC in the chosen day.

We used 6-hr meteorological variables from the fifth generation of the European Center for Medium-Range Weather Forecast atmospheric reanalysis data (ERA5) combined with the ERA5 back extension (BE) (preliminary version) from 1970 to 2021, with a horizontal resolution of $0.25° \times 0.25°$ (Hersbach et al., 2020). To match the timing of daily precipitation observations, we used the records at 12:00 and 18:00 UTC in the previous day and at 00:00 and 06:00 UTC in the chosen day to calculate the daily mean for the ERA5 data set. We also used the National Centers for Environmental Prediction-National Center for Atmospheric Research Reanalysis (NCEP/NCAR; Kalnay et al., 1996) and the Japanese 55-year Reanalysis (JRA-55; Kobayashi et al., 2015) to test the robustness of the large-scale circulation patterns.

The information of tropical cyclone for 1970–2020 is from the best-track tropical cyclone data set compiled by the CMA-Shanghai Typhoon Institute, which provides tropical cyclone locations and intensities at 6-hr intervals. Here, only tropical cyclones reaching tropical depression are considered.

2.2. SOM Methodology

The SOM method projects a nonlinear mapping of a high-dimensional input vector onto a regularly arranged topological low-dimensional (usually two-dimensional) array, where the elements are defined as nodes (Kohonen, 1995), and has been widely used and proved to be effective in characterizing large-scale circulation patterns and identifying their possible impacts on weather and climate extremes (Horton et al., 2015; Li et al., 2020; Tan et al., 2019). For example, Loikith et al. (2017) have connected a series of large-scale circulation patterns, clustered by using SOM, over the northwestern United States with local-scale precipitation and temperature extremes. Swales et al. (2016) examined the role of integrated moisture transport on heavy precipitation events over the U.S. Intermountain West by performing a classification using the SOM.

To represent the large-scale circulation patterns, we use daily anomalies of 500 hPa geopotential height and column-integrated moisture fluxes in the zonal and meridional directions during July–August over the domain 90–150°E, 10–60°N as input for the SOM. The SOM is implemented by the Python miniSOM library (Vettigli, 2021). The technical details have been described in many previous studies (Kim et al., 2021; Kohonen, 2013; Liu et al., 2006; Thompson et al., 2020), here we only provide a brief overview. The number of nodes (clusters) needs to be determined before implementing the SOM, and the Euclidean distance between the initiation nodes (randomly assigned in this study) and each input pattern is calculated to begin the iteration procedure, that is, the "training" of SOM. The winning node is identified by the minimum Euclidean distance, and in the training processes, the winning node and the corresponding neighborhood nodes are updated to be closer to the input pattern. The final SOM nodes are the clustered large-scale circulation patterns. In this study, we have tested several SOM arrays, including 2×3, 3×3, 3×4, 4×4 arrays, and found that a 3×3 node SOM is both sufficient to represent the range of large-scale circulation patterns and easy to distinguish.

2.3. Physical Scaling Diagnostic

Physical scaling diagnostic can be used to decompose changes of extreme precipitation into dynamic and thermodynamic contributions. Following O'Gorman and Schneider (2009) and Pfahl et al. (2017), precipitation amount P_e for daily extreme precipitation at each grid point can be estimated by the scaling relationship, which is expressed as

$$P_e \sim -\left\{ \omega_e \frac{dq_s}{dp}|_{\theta^*} \right\} \tag{1}$$

Here ω_e represents the vertical velocity on the day of extreme precipitation, $dq_s/dp|_{\theta^*}$ is the corresponding vertical derivative of saturation specific humidity q_s with a constant saturation equivalent potential temperature θ^*, and $\{\cdot\}$ is a mass-weighted vertical integration over the troposphere. The right-hand term of Equation 1 represents an estimation of the column-integrated net condensation rate.

In this study, we used the scaling relationship to decompose the differences of precipitation extremes under two circulation patterns, for example, the reference pattern and the changed pattern, to reveal the mechanisms involved in the differences. The thermodynamic contribution (scaling) represents the effect of specific humidity and is estimated using Equation 1 with a constant ω_e (mean value of all days with the occurrence of precipitation extremes under the reference pattern). The dynamic contribution is calculated by subtracting the thermodynamic contribution from the changes in full scaling between the two patterns.

3. Circulation Patterns Most Conducive to Daily Precipitation Extremes in Henan Province

Figure 1d shows the distribution of mean July–August accumulated precipitation over Henan Province for the period 1970–2021. Overall, averaged over the Henan Province, the July–August total precipitation is 300.1 mm, with the maximum values, located to the east of the Funiu Mountain (near 33.5°N, 112.4°E) and to the northwest of the Dabie Mountains (near 31.7°N, 114.8°E), exceeding 400.0 mm. For circulation patterns, during this stage, Henan Province is to the northwest of the western Pacific subtropical high (WPSH), and the tropospheric

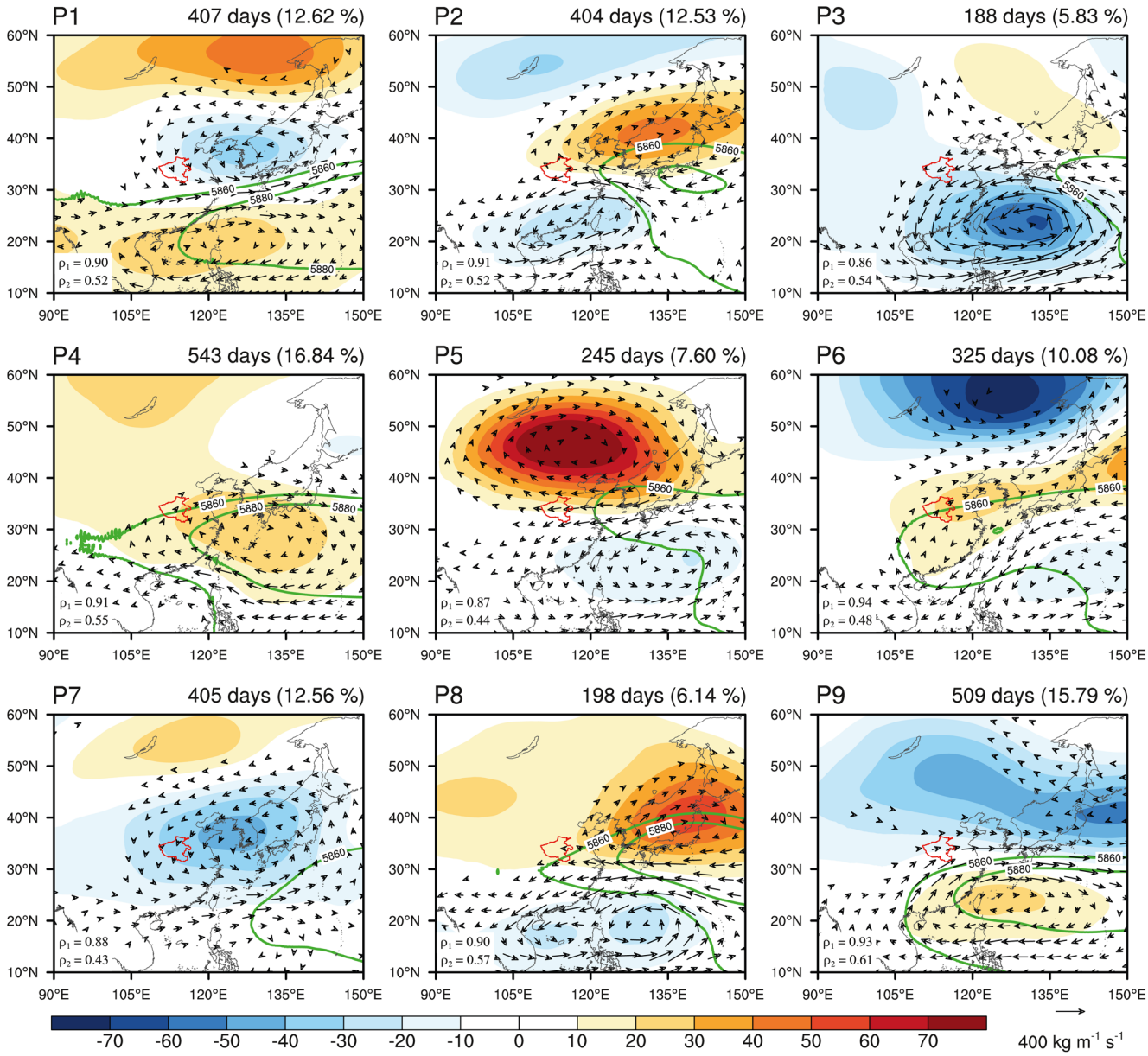

Figure 2. The composite daily anomalies of geopotential height (colored shading, unit: gpm) at 500 hPa and column-integrated moisture flux (arrows; units: $kg \cdot m^{-1} \cdot s^{-1}$) in the 3 × 3 self-organizing map (SOM) nodes. Green lines denote 5,860 and 5,880 gpm contours. The number and occurrence frequency for each pattern are indicated in the upper-right corner. In the lower-left corner, ρ_1 represents the mean pattern correlations for 500 hPa geopotential height between the composite pattern and each pattern in the corresponding SOM node, while ρ_2 is calculated as the average of the two mean pattern correlations for zonal and meridional column-integrated moisture fluxes, respectively.

integrated moisture transport to Henan Province is southwesterly on average from the Bay of Bengal and the South China Sea (Figure 1c), as reported in previous studies (Ding, 1992; Zhou & Yu, 2005).

The nine composites of large-scale circulation patterns, derived using SOM method, are shown in Figure 2. To avoid possible "broadening" or "smearing" problems (Swales et al., 2016), we calculate the averaged pattern correlation coefficient between the composite pattern and each pattern in the corresponding SOM node for all nine patterns. Overall, these mean pattern correlations are statistically significant. For 500 hPa geopotential height, these mean pattern correlations are all greater than 0.85, and for the column-integrated moisture fluxes in zonal and meridional directions, these mean pattern correlations, averaged in two directions, are all greater than 0.40, suggesting that patterns in each node bear high similarities with the mean pattern of that node. Changes in

intensity and position of the WPSH and development of ridges or troughs, relative to the mean state, are manifested by positive or negative height anomalies at 500 hPa. P2, P3, P5 and P8 exhibit similar features, with positive (negative) 500 hPa geopotential height anomalies to the north (south) of Henan Province. And correspondingly, we can observe an evident easterly moisture channel from the western North Pacific to Henan Province. P5 is characterized with the strongest easterly wind anomalies with intense moisture transport in Henan Province among these patterns. Indeed, the mean state southwesterly has been totally replaced by the intensified southeasterly wind under P5 (Figure S1a in Supporting Information S1). Moreover, negative height anomalies to the south of Henan Province are linked to the activities of tropical cyclones. Overall for July–August in 1970–2020, over the western North Pacific west of 150°E, 92.1% of the total 240 days under P5 are observed with activities of tropical cyclones with at least the tropical depression strength (i.e., maximum 2-min sustained wind $\geq$ 10.8 m s^{-1}) based on the best-track tropical cyclone data set.

An opposite anomaly pattern with positive (negative) 500 hPa geopotential height anomalies to the south (north) of Henan Province is seen in P9, which indicates an intensified and westward extended WPSH, strengthening southwesterly moisture transport from the Bay of Bengal and the South China Sea. For P1 and P7, a reduced southwesterly moisture flux (anomaly northerly moisture transport) is observed over Henan Province, accompanied with negative height anomalies centered near the Korean Peninsula. P4 and P6 show positive height anomalies in eastern China associated with anomaly moisture transport from the western North Pacific and the South China Sea. The clustered circulation patterns using NCEP/NCAR and JRA-55 data are largely consistent with the results using ERA5 data combined with ERA5 BE (preliminary version) data (Figures S2 and S3 in Supporting Information S1).

To identify the relationship between circulation patterns and precipitation extremes in Henan Province, for each station, we defined the occurrence frequency of daily precipitation extremes under each circulation pattern as the ratio of the days with precipitation extremes and the total days in that pattern. For example, at Linzhou Station (36.1°N, 113.8°E; triangle in Figure 3), there are 74 days with precipitation exceeding the 95th percentile of precipitation for this station (54.4 mm) during the study period, of which 20 days belong to P5 (245 days in total). Therefore, in P5 the occurrence frequency of daily precipitation extremes is 8.2% at Linzhou Station. The 95th percentile of precipitation on all wet days (with precipitation greater than or equal to 0.1 mm) is used as the main threshold for precipitation extremes. Figure 3 shows the spatial distribution of occurrence frequency of daily precipitation extremes and the proportions of stations with occurrence frequencies exceeding different thresholds, that is, the 2.0%, 3.0%, 4.0% and 5.0%, under each circulation pattern. A striking feature is that the largest proportion of stations with high occurrence frequency in daily precipitation extremes is seen under P5 (Figure 3b). For example, the proportion of stations with precipitation extremes occurrence frequency exceeding 3.0% in P5 is 49.1%, far larger than those in other circulation patterns. The high occurrence frequency under this pattern mainly concentrates over central and northern Henan Province, exactly the windward slope of the Taihang Mountains and the Funiu Mountain for easterly flow, where the occurrence of extreme precipitation is orographically enhanced (Ding, 2015; Ran et al., 2021; Zhang et al., 2021). P9 ranks second in the proportion (29.5%) of stations with high occurrence frequency (>3%) of precipitation extremes among all circulation patterns. The higher occurrence frequency of precipitation extremes under P9 is mainly distributed over the southeast Henan Province, coinciding with the high rainfall region in the climatology (Figure 1d).

In addition to the frequency assessment, we investigated the mean intensities of precipitation extremes with different thresholds, that is, the 90th, 95th, 98th, and 99th percentiles of precipitation on all wet days. This is done by averaging all daily precipitation extremes for all stations in Henan Province under each circulation pattern. As shown in Figure S4 in Supporting Information S1, precipitation extremes under P5 is also featured with the largest mean intensity. For example, the mean intensity for daily precipitation extremes with the 99th percentile threshold is 169.6 mm, at least 45% larger than those in other circulation patterns. Therefore, though P5 only accounts for a low percentage (7.60%) among all nine patterns, it is the circulation pattern most conducive to the occurrence of precipitation extremes. Indeed, seven out of total 11 days in the "21·7" and the "75·8" extraordinary rainfall events belong to P5, and the top two maximum hourly precipitation extremes over continental China occurred under P5.

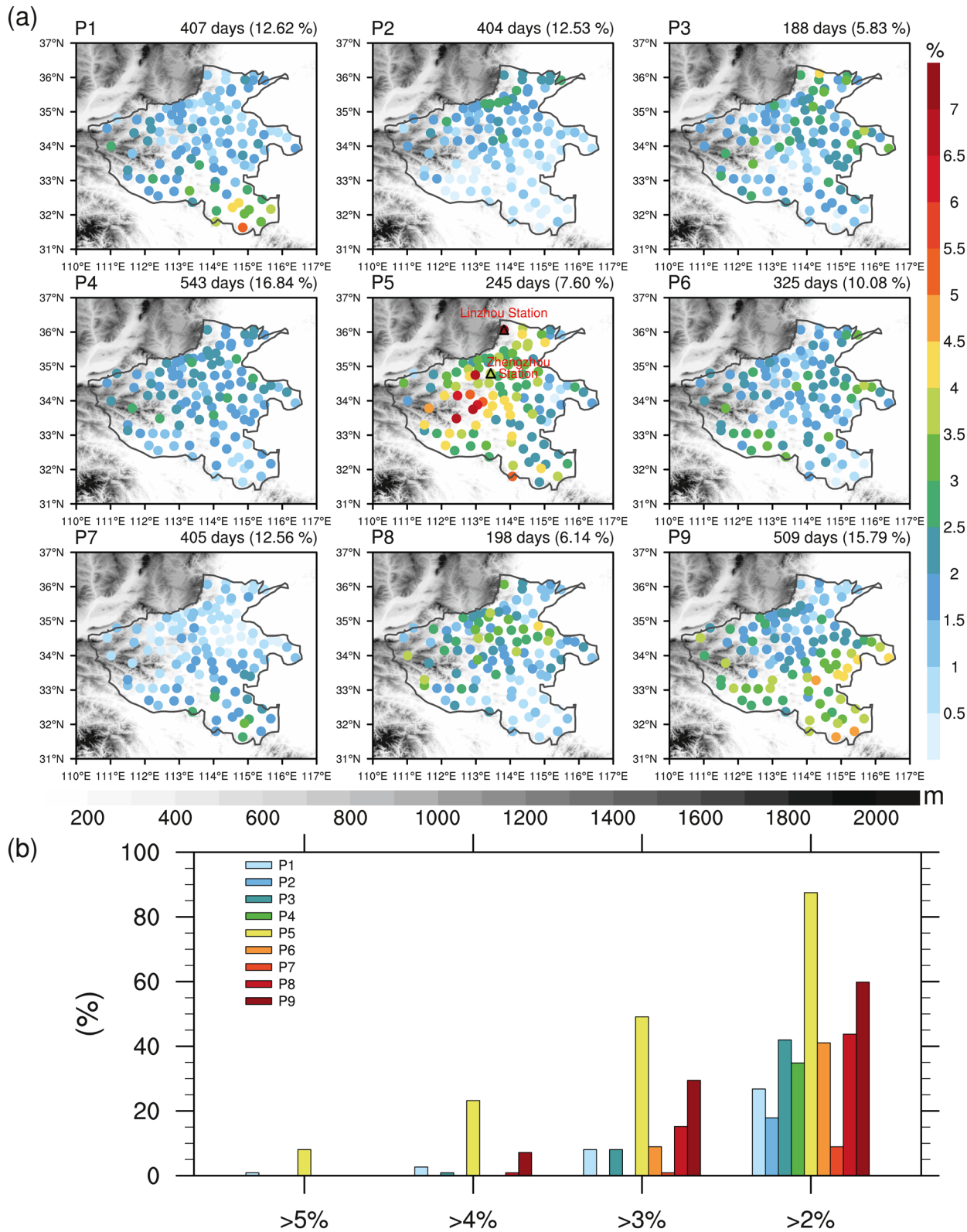

Figure 3. (a) Spatial distribution of the occurrence frequency (colored dots; units: %) of daily precipitation extremes with the threshold of 95th percentile in the 3 × 3 self-organizing map (SOM) nodes. (b) Distribution of proportions (units: %) of stations with occurrence frequency exceeding 2.0%, 3.0%, 4.0% and 5.0% in each SOM node.

4. Why Are the Daily Precipitation Extremes Under P5 Most Intense?

The above analysis shows that daily precipitation extremes occur with the highest frequency and the largest mean intensity under P5. In this section we intend to reveal the mechanisms at play by comparing precipitation extremes between P5 and the rest eight patterns based on the ERA5 data. The spatial distribution of mean intensity of daily precipitation extremes in the 3 × 3 SOM nodes based on the ERA5 data (Figure S5 in Supporting Information S1) is largely consistent with the results based on the observational precipitation data. As indicated in Figure S6 in Supporting Information S1, the full scalings, based on Equation 1, bear high similarities with the corresponding precipitation extremes directly from the ERA5 data, with spatial correlation coefficients all greater than 0.8 under all nine circulation patterns, proving the effectiveness of the scaling relationship.

To shed light on the reason why the mean intensity for precipitation extremes under P5 is the largest, we decompose the changes of precipitation extremes, between P5 and all eight other patterns, into thermodynamic and dynamic contributions. The spatial distribution of the changes in extreme precipitation exceeding the 95th percentile agrees well with the corresponding full scaling (Figures 4a and 4b). For extreme precipitation exceeding the 95th percentile, the fractional difference of thermodynamic scaling between P5 and other patterns is relatively small in amplitude (lower than 5%) over Henan Province (Figure 4c). In contrast, fractional changes in dynamic scaling are consistently positive over most regions of Henan Province and exhibit a pronounced regional difference (Figure 4d). Note that the changes in dynamic and thermodynamic scaling are corresponding to those of vertical velocity ω_e and vertically integrated saturation specific humidity q_s on the days of extreme precipitation (Figure S7 in Supporting Information S1), respectively. Averaged over Henan Province, the increases in the dynamic scaling dominate the increases in full scaling between P5 and all eight other patterns, for precipitation extremes exceeding the 90th, 95th, 98th and 99th percentiles, while the contributions of the thermodynamic scaling are small (Figure 4e). Therefore, we could safely conclude that the stronger ascending motions are primarily responsible for the larger mean intensity for precipitation extremes under P5. Moreover, the difference of thermodynamic and dynamic scaling between P9 and other patterns is shown in Figure S8 in Supporting Information S1. The thermodynamic contribution dominated the increase in extreme precipitation exceeding the 95th percentile between P9 and other patterns, which corresponds to the strengthening southwesterly moisture transport from the Bay of Bengal and the South China Sea in P9.

5. Conclusions and Discussion

In this study, we applied SOM clustering method to identify nine large-scale circulation patterns for July–August in Henan, one of the most populated provinces in China. We find that the P5 is most conducive to daily precipitation extremes, showcasing the highest frequency and intensity of precipitation extremes among all nine patterns. Seven out of total 11 days for the "21·7" and the "75·8" events belong to P5, and the top two maximum hourly precipitation extremes over continental China occurred under P5. In this pattern, the Henan Province is exactly to the windward slope of the strong easterly flow anomalies associated with tropical cyclone activity over the western North Pacific. Using a physical scaling method, we decomposed the differences in precipitation extremes between P5 and the other patterns into dynamical and thermodynamical contributions. The larger mean intensity for precipitation extremes under P5 is mainly attributed to the dynamics, that is, the stronger ascending motions, with relatively little contribution from the thermodynamics, that is, the moisture conditions. The dynamic effect may have been mainly related to the strong mid to low-troposphere easterly wind, the peculiar terrain (the Taihang Mountains and the Funiu Mountain) to the west of the province and the so-called train effect with the development and movement of multi-cell storms, and the maintenance of mesoscale convergence line in eastern Henan (Ding, 2015; Zhang et al., 2021).

Indeed, previous studies also emphasized that strong ascending motions induced by topographical lifting are critical to the development of the "21·7" and the "75·8" extreme precipitation events (Ding, 2015; Zhang et al., 2021). However, few studies used the SOM clustering method to study the circulation patterns associated with such catastrophic extreme precipitation events. Moreover, we have, in a quantitative manner, clarified the dominant role of the stronger ascending motion in the stronger precipitation extremes in P5 circulation pattern. It should be noted that both catastrophic extreme rainfall events, that is, the "75·8" and "21·7" events, are the result of extremely favorable and complicated circulation configurations. As shown in previous studies (Ding, 2015; Ran et al., 2021), the "75·8" and "21·7" events are associated with a landfall TC over South China and a remote TC

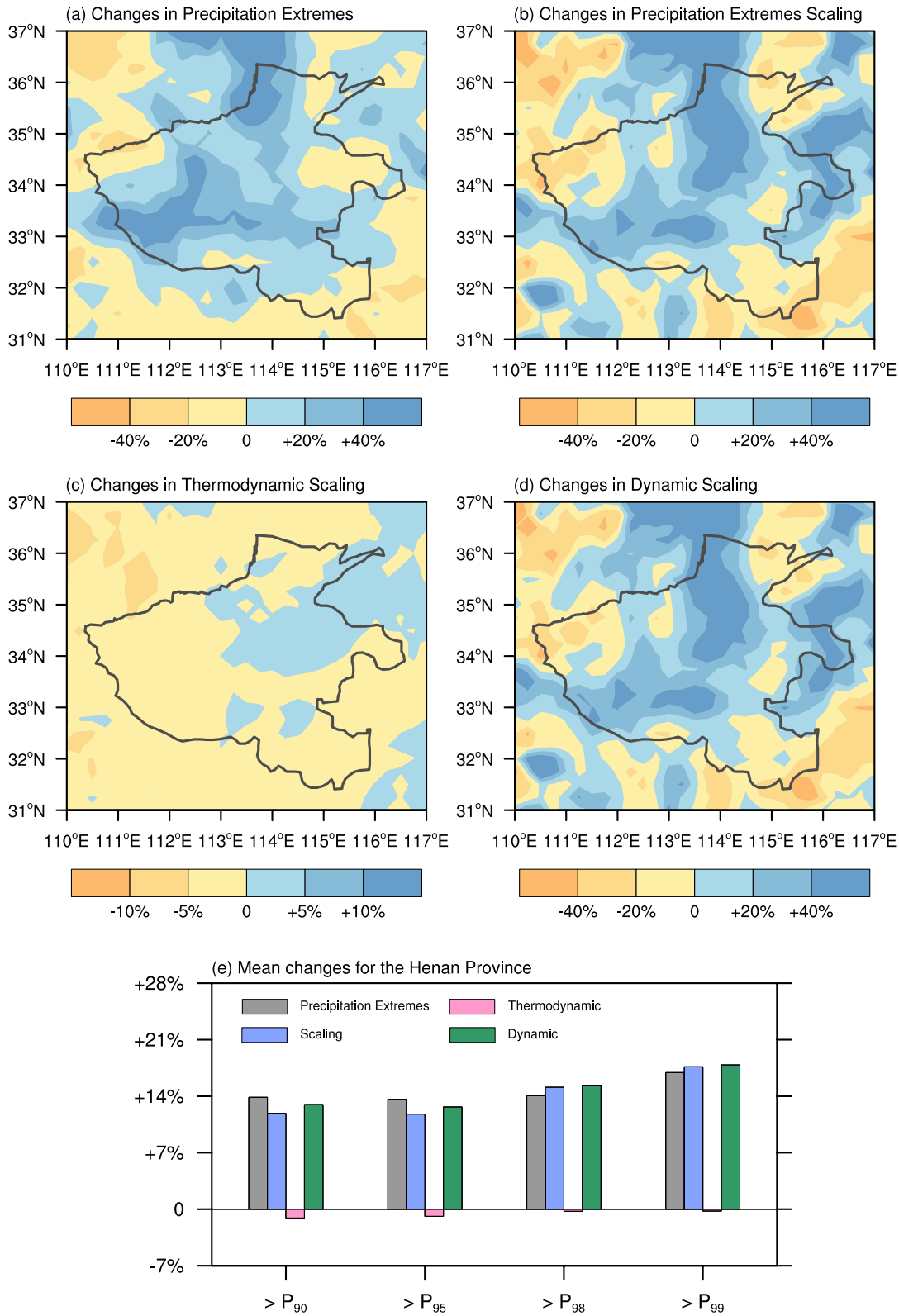

Figure 4. Fractional changes of P5 relative to other patterns in mean (a) precipitation extremes, (b) full scaling, (c) thermodynamic scaling, and (d) dynamic scaling for all days with daily precipitation exceeding the 95th percentile. (e) Regional mean changes of P5 relative to other patterns over the Henan Province in precipitation extremes, full scaling, thermodynamic scaling, and dynamic scaling for all days with daily precipitation exceeding the 90th, 95th, 98th, and 99th percentiles.

over the western North Pacific, respectively. Both are featured with a north-south dipole structure of anomalies in 500 hPa geopotential height and an anomaly easterly wind (Figure S1 in Supporting Information S1). We further decompose the differences of precipitation extremes, between the 7 days of the two extreme rainfall events under P5 and all the other days, into thermodynamic and dynamic contributions (Figure S9 in Supporting Information S1). The more intensified precipitation of the two catastrophic extreme rainfall events, relative to the rest days, is dominated by the dynamic contribution, while the thermodynamic effect shows no obvious difference between them. Indeed, several variables are certainly not enough to represent all characteristic features of these two events. Other variables such as specific humidity, vertical velocity, low-level wind (Ohba et al., 2015; Schlef et al., 2019) could be integrated to sufficiently and effectively represent the large-scale weather patterns.

This study provides a meaningful step in linking the occurrence of precipitation extremes in Henan Province with large-scale conditions. We provide a framework, combining the SOM clustering method with the physical scaling diagnostic, to identify the circulation pattern most conducive to precipitation extremes and to reveal the involved mechanism by decomposing precipitation extremes changes into thermodynamic and dynamic contributions. In this way, we could investigate many aspects of precipitation extremes, including evaluating how well global climate models simulate these large-scale circulation patterns and their relationship to precipitation extremes, and assessing their past and future changes.

Data Availability Statement

Due to the data policy in China, the original climate records of precipitation at the 2,425 stations are not available via a website for the public. However, anyone could contact the China Meteorological Data Service Center (http://data.cma.cn/en) or the China Meteorological Administration (CMA) (http://www.cma.gov.cn/en2014/aboutcma/contactus/) for detailed information on data acquisition. The processed precipitation data are available at http://data.cma.cn/sj/dataPub/dataDetail.html?dataCode=292. The meteorological data are retrieved from the ERA5 by the European Center for Medium-Range Weather Forecast at https://www.ecmwf.int/en/forecasts/datasets/reanalysis-datasets/era5. Population counts are from the Gridded Population of the World Version 4 database at http://sedac.ciesin.columbia.edu/data/collection/gpw-v4. The intensity and best-track data of typhoons were obtained from CMA tropical cyclone database (https://tcdata.typhoon.org.cn/en/zjljsjj_zlhq.html). The self-organizing map is implemented by the Python miniSOM library (Vettigli, 2021).

Acknowledgments
This work was supported by the National Key R&D Program of China (2018YFA0605604) and the Proyecto Corfo Ingeniería 2030 código (14ENI2-26865).

References

Chang, M., Liu, B., Martinez-Villalobos, C., Ren, G., Li, S., & Zhou, T. (2020). Changes in extreme precipitation accumulations during the warm season over continental China. *Journal of Climate*, *33*(24), 10799–10811. https://doi.org/10.1175/JCLI-D-20-0616.1

Chang, M., Liu, B., Wang, B., Martinez-Villalobos, C., Ren, G., & Zhou, T. (2021). Understanding future increases in precipitation extremes in global land monsoon regions. *Journal of Climate*, *35*(6), 1839–1851. https://doi.org/10.1175/JCLI-D-21-0409.1

Chen, Z., & Zhang, J. (2020). The characteristics of late summer extreme precipitation in northern China and associated large-scale circulations. *International Journal of Climatology*, *40*(12), 5170–5187. https://doi.org/10.1002/joc.6512

Ding, Y. (1992). Summer monsoon rainfalls in China. *Journal of the Meteorological Society of Japan*, *70*, 373–396. https://doi.org/10.2151/jmsj1965.70.1B_373

Ding, Y. (2015). On the study of the unprecedented heavy rainfall in Henan Province during 4–8 August 1975: Review and assessment. *Acta Meteorologica Sinica*, *73*, 411–424. https://doi.org/10.11676/qxxb2015.067

Ding, Y., & Chan, J. C. L. (2005). The East Asian summer monsoon: An overview. *Meteorology and Atmospheric Physics*, *89*(1–4), 117–142. https://doi.org/10.1007/s00703-005-0125-z

Ding, Y., Li, J., & Sun, S. (1980). The analysis on mesoscale systems producing heavy rainfall in North China. *Papers of Institute of Atmospheric Physics, Chinese Academy of Sciences*, *9*, 1–13.

Ding, Y., & Zhang, J. (2009). *Rainstorm and flood*. Meteorological Press.

Hersbach, H., Bell, B., Berrisford, P., Hirahara, S., Horányi, A., Muñoz-Sabater, J., et al. (2020). The ERA5 global reanalysis. *Quaterly Journal of the Royal Meteorological Society*, *146*(730), 1999–2049. https://doi.org/10.1002/qj.3803

Horton, D., Johnson, N., Singh, D., Swain, D. L., Rajaratnam, B., & Diffenbaugh, N. S. (2015). Contribution of changes in atmospheric circulation patterns to extreme temperature trends. *Nature*, *522*(7557), 465–469. https://doi.org/10.1038/nature14550

Kalnay, E., Kanamitsu, M., Kistler, R., Collins, W., Deaven, D., Gandin, L., et al. (1996). The NCEP/NCAR 40-year reanalysis project. *Bulletin of the American Meteorological Society*, *77*(3), 4372–472. https://doi.org/10.1175/1520-0477(1996)077<0437:tnyrp>2.0.co;2

Kim, H. K., Moon, B. K., Kim, M. K., Park, J. Y., & Hyun, Y. K. (2021). Three distinct atmospheric circulation patterns associated with high temperature extremes in South Korea. *Scientific Reports*, *11*(1), 12911. https://doi.org/10.1038/s41598-021-92368-9

Kobayashi, S., Ota, Y., Harada, Y., Ebita, A., Moriya, M., Onoda, H., et al. (2015). The JRA-55 Reanalysis: General specifications and basic characteristics. *Journal of the Meteorological Society of Japan*, *93*(1), 5–48. https://doi.org/10.2151/jmsj.2015-001

Kohonen, T. (1995). *Self-organizing maps*. Springer.

Kohonen, T. (2013). Essentials of the self-organizing map. *Neural Networks*, *37*, 52–65. https://doi.org/10.1016/j.neunet.2012.09.018

Li, M., Jiang, Z., Zhou, P., Le Treut, H., & Li, L. (2020). Projection and possible causes of summer precipitation in eastern China using self-organizing map. *Climate Dynamics*, *54*(5), 2815–2830. https://doi.org/10.1007/s00382-020-05150-4

Liu, Y., Weisberg, R. H., & Mooers, C. N. K. (2006). Performance evaluation of the self-organizing map for feature extraction. *Journal of Geophysical Research*, *111*(C5), C05018. https://doi.org/10.1029/2005JC003117

Loikith, P. C., Lintner, B. R., & Sweeney, A. (2017). Characterizing large-scale meteorological patterns and associated temperature and precipitation extremes over the northwestern United States using self-organizing maps. *Journal of Climate*, *30*(8), 2829–2847. https://doi.org/10.1175/JCLI-D-16-0670.1

Luo, Y., Wu, M., Ren, F., Li, J., & Wong, W. (2016). Synoptic situations of extreme hourly precipitation over China. *Journal of Climate*, *29*(24), 8703–8719. https://doi.org/10.1175/JCLI-D-16-0057.1

O'Gorman, P. A., & Schneider, T. (2009). Scaling of precipitation extremes over a wide range of climates simulated with an idealized GCM. *Journal of Climate*, *22*(21), 5676–5685. https://doi.org/10.1175/2009JCLI2701.1

Ohba, M., Kadokura, S., Yoshida, Y., Nohara, D., & Toyoda, Y. (2015). Anomalous weather patterns in relation to heavy precipitation events in Japan during the Baiu season. *Journal of Hydrometeorology*, *16*(2), 688–701. https://doi.org/10.1175/JHM-D-14-0124.1

Pfahl, S., O'Gorman, P., & Fischer, E. (2017). Understanding the regional pattern of projected future changes in extreme precipitation. *Nature Climate Change*, *7*(6), 423–427. https://doi.org/10.1038/nclimate3287

Ran, L., Li, S., Zhou, Y., Yang, S., Ma, S., Zhou, K., et al. (2021). Observational analysis of the dynamic, thermal, and water vapor characteristics of the "7.20" extreme rainstorm event in Henan province, 2021. *Chinese Journal of Atmospheric Sciences*, *45*(6), 1366–1383. https://doi.org/10.3878/j.issn.1006-9895.2109.21160

Schlef, K., Moradkhani, H., & Lall, U. (2019). Atmospheric circulation patterns associated with extreme United States floods identified via machine learning. *Scientific Reports*, *9*(1), 7171. https://doi.org/10.1038/s41598-019-43496-w

Shi, W., Li, X., Zeng, M., Wang, H., Zhu, K., & Zhu Ge, X. (2021). Multi-model comparison and high-resolution regional model forecast analysis for the "7·20" Zhengzhou severe heavy rain. *Transactions of Atmospheric Sciences*, *44*(5), 688–702. https://doi.org/10.13878/j.cnki.dqkxxb.20210823001

Sun, J., He, N., Wang, G., Chen, M., Liao, X., & Wang, H. (2012). Preliminary analysis on synoptic configuration evolvement and mechanism of a torrential rain occurring in Beijing on 21 July 2012. *Torrential Rain and Disasters*, *31*(3), 218–225. https://doi.org/10.3969/j.issn.1004-9045(2012)03-0218-08

Swales, D., Alexander, M., & Hughes, M. (2016). Examining moisture pathways and extreme precipitation in the U.S. Intermountain West using self-organizing maps. *Geophysical Research Letters*, *43*(4), 1727–1735. https://doi.org/10.1002/2015GL067478

Tan, X., Gan, T. Y., Chen, S., Horton, D. E., Chen, X., Liu, B., & Lin, K. (2019). Trends in persistent seasonal-scale Atmospheric circulation patterns responsible for seasonal precipitation totals and occurrences of precipitation extremes over Canada. *Journal of Climate*, *32*(21), 7105–7126. https://doi.org/10.1175/JCLI-D-18-0408.1

Thompson, H. D., Déry, S. J., Jackson, P. L., & Laval, B. E. (2020). A synoptic climatology of potential seiche-inducing winds in a large intermontane lake: Quesnel Lake, British Columbia, Canada. *International Journal of Climatology*, *40*(14), 5973–5986. https://doi.org/10.1002/joc.6560

Vettigli, G. (2021). *Minisom*. Retrieved from https://github.com/JustGlowing/minisom

Wu, M., & Luo, Y. (2019). Extreme hourly precipitation over China: Research progress from 2010 to 2019. *Torrential Rain and Disasters*, *38*(5), 502–514. https://doi.org/10.3969/j.issn.1004-9045.2019.05.012

Xia, R., & Zhang, D. (2019). An observational analysis of three extreme rainfall episodes of 19–20 July 2016 along the Taihang Mountains in North China. *Monthly Weather Review*, *147*(11), 4199–4220. https://doi.org/10.1175/MWR-D-18-0402.1

Zhang, X., Yang, H., Wang, X., Shen, L., Wang, D., & Li, H. (2021). Analysis on characteristic and abnormality of atmospheric circulations of the July 2021 extreme precipitation in Henan. *Transactions of Atmospheric Sciences*, *44*(5), 672–687. https://doi.org/10.13878/j.cnki.dqkxxb.20210907001

Zhao, Y., Xu, X., Li, J., Zhang, R., Kang, Y., Huang, W., et al. (2019). The large-scale circulation patterns responsible for extreme precipitation over the North China plain in midsummer. *Journal of Geophysical Research: Atmospheres*, *124*(23), 12794–12809. https://doi.org/10.1029/2019JD030583

Zhou, T., & Yu, R. (2005). Atmospheric water vapor transport associated with typical anomalous summer rainfall patterns in China. *Journal of Geophysical Research*, *110*, D08104. https://doi.org/10.1029/2004JD005413